Colloids and Surfaces A: Physicochem. Eng. Aspects 357 (2010) 74–83

Contents lists available at ScienceDirect

Colloids and Surfaces A: Physicochemical and Engineering Aspects

journal homepage: www.elsevier.com/locate/colsurfa

A study of the pore size distribution for activated carbon monoliths and their relationship with the storage of methane and hydrogen

A.A. García Blanco [a], J.C. Alexandre de Oliveira [a], R. López [a], J.C. Moreno-Piraján [b], L. Giraldo [c], G. Zgrablich [a], K. Sapag [a,*]

[a] Instituto de Física Aplicada-CONICET, Dpto. de Física, Universidad Nacional de San Luis, Chacabuco 917, CP: 5700, San Luis Capital, San Luis, Argentina
[b] Dpto. de Química, Universidad de los Andes, Bogotá, Colombia
[c] Dpto. de Química, Universidad Nacional de Colombia, Bogotá, Colombia

ARTICLE INFO

Article history:
Received 2 July 2009
Received in revised form 5 January 2010
Accepted 5 January 2010
Available online 15 January 2010

Keywords:
Methane storage
Pore size distribution
GCMC simulation

ABSTRACT

By adsorption of different gases and simulation methods it was studied the characterization of microporous monoliths in activated carbons from coconut shells in relation to the storage capacity of gases that present energetic interest. Adsorption isotherms of nitrogen, methane, carbon dioxide and hydrogen at different temperatures were measured at sub-atmospheric pressures. Additional adsorption isotherms of methane were performed at room temperature and high pressures (up to 4.5 MPa). A Grand Canonical Monte Carlo simulation of adsorption on slit pores was carried out for these gases. The simulated data were adjusted to experimental data to optimize the models. Different parameters such as micropore volume, pore size distribution and differential isosteric enthalpy of adsorption, were studied and related to the hydrogen and methane storage capacity for these materials.

1. Introduction

Natural gas is considered as an appropriate alternative fuel due to its huge resource, low price and low toxic gas emission. However, natural gas requires a special storage system due to its low volumetric energy density [1]. It is also known that the adsorbed natural gas (ANG) storage system is a feasible process, which can solve several problems in storing natural gas [2–4]. ANG is a method where both adsorption and compression processes are simultaneously carried out to store natural gas under convenient temperature and pressure compared to the conventional methods [5]. The best adsorbents to be used in this process are those with pores in the microporous range, where activated carbon (AC) has been extensively used [6,7] with good results. In general, the adsorption of methane on AC is studied as a representative gas for the ANG storage in porous materials. In these studies the most common parameters used to measure the efficiency of AC as a storage medium is the amount of methane adsorbed per volume unit of the container, which increases with the micropore volume and the bulk density of the carbon [8]. A binder less consolidated disc or monolithic activated carbon without loss of micropore volume is preferred to traditional granular activated carbon because it can be manufactured with higher bulk density and can be adapted to the shape of the container [9,10]. The characteristics of the microporous materials are closely related to the methane adsorption capacity, since numerous studies agree on the fact that this quantity is favored by high surface area (>1000 $m^2\,g^{-1}$), high micropore volume and average pore size within the range of 8–15 Å. In general, these properties are obtained by measuring the nitrogen and carbon dioxide adsorption isotherms, which are analyzed by using different models or methods [11–14].

In addition to methane, in the last years hydrogen has been accepted as a new gas with some advantages for energetic applications. Nevertheless, its storage is the main problem to be conquered for the successful implementation of the fuel cell technology in transport applications and it represents a major challenge in the material science. The use of hydrogen physisorption in porous materials, in particular AC, is one of the main methods to be considered for convenient gas storage. Several articles [15–19] introduce the use of AC to store hydrogen in different conditions, where the textural characteristics like porosity, surface area and differential heat of adsorption play an important role. A recent work [20], based on the use of a thermodynamical model of hydrogen storage in slit pores, predicts that the optimum average pore size to reach the hydrogen storage targets for 2010, established by the US Department of Energy, should be within the range of 5–6 Å.

Then, for both processes, methane and hydrogen storage, the key for the success in finding an efficient storage system is the selection of a suitable adsorbent. In such a selection the characterization of the porous texture of the material plays a relevant role.

The pore structure of porous materials is usually described in terms of the pore size distribution (PSD) and several methods were

* Corresponding author. Tel.: +54 2652436151; fax: +54 2652436151.
E-mail address: sapag@unsl.edu.ar (K. Sapag).

0927-7757/$ – see front matter © 2010 Elsevier B.V. All rights reserved.
doi:10.1016/j.colsurfa.2010.01.006

developed for the PSD analysis, where the most accepted methodologies are the density functional theory (DFT) [21–23] and the Monte Carlo (MC) simulation [24,25]. The first is based on a mean-field approximation of fluid–fluid attraction, which may become inaccurate for fluids confined within very small pores. The second one models actual molecular microscopic configurations of the confined fluid using realistic intermolecular interaction potentials and, in principle within statistical errors, provides exact predictions for the used potentials [24].

The aim of this work is to synthesize AC monoliths, characterize them obtaining their PSDs and relate their textural characteristics to their methane and hydrogen storage capacity.

A central problem in the characterization of AC is the accurate determination of the PSD from adsorption isotherm of a probe molecule, usually N_2 at 77 K. However, in many microporous networks very slow adsorption processes are observed and such diffusion limitations can lead to significant underestimation of the adsorption isotherm [26], especially for the ultra-micropores (<7 Å) rich samples. Adsorption measurements at higher temperatures represent a more convenient alternative in terms of both experimental time and precision [27]. For instance CO_2 has been extensively used at 273 K, because it can easily access micropores which would present diffusion resistance for N_2 at 77 K [28]. At this temperature, CO_2 molecules can more easily access ultra-micropores than N_2 at 77 K in spite of the fact that critical molecular dimensions of both gases are similar. Other gases, like H_2, were also employed to obtain information about carbon microporosity [29]. Then, the selection of the probe molecule to be used in the analysis of the pore structure should be careful, because different gases explore different ranges of pore size [30,31].

Any method for the determination of the PSD begins with the proposition of a model to represent the relevant geometric and structural characteristics of the porous material. It is important to stress the fact that such a model is not intended to mimic the real porous structure, but it is rather an idealization intended to reproduce with a maximum degree of accuracy the adsorption properties of the material. The slit model, which represents the material as a collection of slit geometry pores of different sizes, is usually assumed for the characterization of AC and has been extensively used in determining the PSD [32–37]. We have adopted the slit-shaped pore model since it not only represents a physically plausible pore shape but it is also the simplest pore model that can fit the experimental data for adsorption on carbons [38].

In this work we report, on one hand, the experimental adsorption isotherms of N_2 and H_2 at 77 K, of CO_2 at 273 K and of CH_4 at 298 K, at low pressure, and adsorption isotherms of methane at 298 K, at high pressures, in AC monoliths obtained from coconut shells. On the other hand, we introduce the results of the respective Grand Canonical Monte Carlo (GCMC) simulation method in the continuum space for individual slit-shaped graphitic pores of varying width ranging from 1 to 12 molecular diameters. The experimental and theoretical data were used in order to derive individual PSDs [39] (one for each experimental isotherm) of ACs. We discuss the implications of these results for material characterization procedures based on gas adsorption data. Finally, we relate the textural properties of activated carbons to their gas storage capacity for methane and hydrogen.

The remainder of this paper is divided into the following sections. First, we report the experimental research of the system. The next section deals with modeling the adsorption of the components in slit pores using molecular simulation. The last section presents results, fits and predictions on the basis of these PSDs in comparison to experimental results and also discusses the limits of applicability of this approach.

2. Experimental

2.1. Sample preparation

The AC monoliths were obtained by chemical activation of coconut shells with zinc chloride [40,41]. The granular precursor (particle size <38 μm) was added to a solution of $ZnCl_2$ with a concentration of 40 wt%, and impregnated through 7 h at 85 °C. Then, the temperature was increased to evaporate the solution until dryness. The impregnated particles were compacted and conformed under pressure (150 MPa) in a cylindrical mould at 150 °C into discs with 2 cm diameter. The resulting discs were heated in a horizontal furnace (Thermolyne T9300 with a quartz reactor 30 cm long and 4 cm internal diameter) at a heating rate of 2 °C min^{-1} up to 500 °C and a soaking time of 1 h, in a nitrogen flow of 100 ml min^{-1}. The carbonized discs were washed with a diluted solution of hydrochloric acid and then with distilled water until no chloride ions were detected (checked with the silver nitrate test). After this, the discs were dried in an oven at 110 °C in air and these samples were denominated M40. Two of the carbonized discs were further heated in the horizontal furnace under a nitrogen flow up to 800 °C and then, physically activated with carbon dioxide at 800 °C in a flow of 150 ml min^{-1}, with soaking times of 3 h (developing a 20% burn-off, monolith M40-20) or 5 h (developing a 28% burn-off, monolith M40-28) in order to improve their microporosity.

2.2. Characterization

The characterization of the samples was performed by gas adsorption of different gases. Adsorption isotherms of nitrogen (99.999% purity) at 77 K and carbon dioxide (99.996% purity) at 298 K were measured in a volumetric system Autosorb AS-1MP (Quantachrome Instruments). Hydrogen (99.995% purity) isotherms at 77 K and pressures below 0.1 MPa were measured in a volumetric system ASAP 2000 (Micromeritics Instrument Corporation). High pressure adsorption isotherms of methane (99.995% purity) were measured up to 4.5 MPa at 298 K in a high pressure volumetric system HPA 100 (VTI Corporation, currently TA Instruments). Previous to all the adsorption experiments, the samples were degassed at 250 °C during 8 h under vacuum conditions (5×10^{-3} mmHg). The micropore volume (Vmp) was calculated by application of the Dubinin–Radushchevich (DR) equation to the adsorption data for N_2 and CO_2 [42], and by the application of the α_s-plot method to the adsorption data for N_2, using the reference isotherm for non-porous carbon [43].

3. Molecular simulation of the adsorption of pure component in model pores

The most widely used molecular simulation method applied to adsorption problems is the GCMC because it allows a direct calculation of the phase equilibrium between a gas phase and an adsorbed phase. The implementation of this simulation method is both well established and well documented [44,45].

In this work, all the gases were modeled as a one-center Lennard–Jones (LJ) interaction site. With this supposition we could reproduce bulk fluid experimental coexistence data for each adsorbate with reasonable accuracy. Clearly, for more demanding problems more accurate interaction potentials are required.

The gas–gas potential was taken as the usual Lennard–Jones potential:

$$U_{gg}(r) = -4\varepsilon_{gg}\left[\left(\frac{\sigma_{gg}}{r}\right)^6 - \left(\frac{\sigma_{gg}}{r}\right)^{12}\right] \quad (1)$$

Table 1
Parameters used in the GCMC simulations.

Molecule	σ_{gg} (nm)[a]	ε_{gg}/k_B (K)[a]	σ_{gs} (nm)[b]	ε_{gs}/k_B (K)[c]	Ref.
CO_2	0.3750	236.1	0.3590	81.3	[46]
CH_4	0.3821	148.2	0.3625	64.4	[49]
H_2	0.2960	34.2	0.3195	30.9	[46]
N_2	0.3615	101.6	0.3494	56.3	[47]
Carbon	0.3400	28.0	–	–	[46]

[a] Lennard–Jones parameters.
[b] Lorentz–Berthelot rules (except N_2).
[c] Boltzman constant: $k_B = 1.380/650424 \times 10^{-23}$ (J/K).

where ε_{gg} and σ_{gg} are the energetic and geometrical parameters of the LJ potential and r is the intermolecular separation.

The gas–solid potential for the slit geometry is given by the superposition of two Steele potentials [45], one per each infinite plate:

$$U_{\text{gs-STEELE}}(z) = 2\pi\varepsilon_{gs}\rho_C\sigma_{gs}^2\Delta \times \left\{\frac{2}{5}\left(\frac{\sigma_{gs}}{z}\right)^{10} + \left(\frac{\sigma_{gs}}{z}\right)^4 - \frac{\sigma_{gs}^4}{3\Delta(z+0.61\Delta)^3}\right\} \qquad (2)$$

where Δ is the separation between layers in graphite (0.335 nm) [46], ρ_C is the number of carbon atoms per unit volume of graphite (114 nm^{-3}) [46], z is the distance from the center of a gas molecule to the nuclei of the carbon atoms in the surface graphitic plane, ε_{gs} and σ_{gs} are the LJ parameters for the interaction between a gas molecule and a graphite carbon atom.

The values of the parameters included in the interaction potentials (Eqs. (1) and (2)) are given in Table 1 [46–49], where the parameter σ represents the LJ collision diameter, being σ_{gg} for the gas and σ_{ss} for carbon. The cross LJ parameters (arithmetic mean for collision diameter, $\sigma_{gs,}$ and geometric mean for well depth ε_{gs}) were determined using the standard Lorentz–Berthelot combining rules.

Data bases of adsorption isotherms (the local isotherms, θ_L) were calculated for nitrogen, hydrogen, methane and carbon dioxide, for a range of pressures, pore widths and temperatures through the GCMC method, following the algorithm outlined in Ref. [50]. Transition probabilities for each Monte Carlo attempt, displacement, adsorption and desorption of molecules, are given by the usual Metropolis rules. The lateral dimensions of the cell for the slit geometry were taken as L = 10.3 nm and periodic boundary conditions were used in these directions. The cutoff distance, beyond which the potential gas-gas is neglected, is set to be $5\sigma_{gg}$. Equilibrium was generally achieved after 10^7 MC attempts, after which mean values were taken over the following 10^7 MC attempts for configurations spaced by 10^3 MC attempts in order to ensure statistical independence. A MC step is an attempted translation, creation, or destruction of a molecule.

At defined temperature and pressure, the calculations were performed by using the state equation for ideal gases at low pressure (up to 0.1 MPa) and the Peng–Robinson [51] equation of state for high pressure, where the parameters used are shown in Table 2 [52–54].

The actual quantity calculated in our GCMC simulations is the absolute adsorption density, i.e. the average number of molecules

Table 2
Critical constants used in the Peng–Robinson equation of state for methane.

Critical temperature (K)	190.6
Critical pressure (bar)	45.99
Accentricity factor	0.012

Critical parameters from Refs. [52,54].

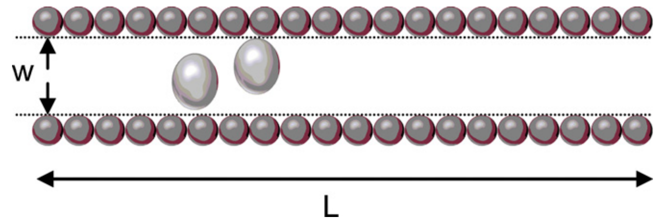

Fig. 1. Model of the slit pore used in the simulation.

of each gas at determined pressure, per pore volume. In Fig. 1 a scheme of the used slit pore model is presented, where w represents the pore width, L the lateral dimension of the pore and the pore volume is $L \times L \times w$.

In order to compare theoretical with experimental adsorption isotherms, the absolute adsorption obtained by GCMC simulation was converted to excess adsorption, the quantity determined by experimental measurements, by using a bulk equation of state to determine the number of molecules that would have been present in absence of adsorbate–adsorbent interaction. The conversion was carried out using:

$$n_{ex}(w, P) = n_{abs}(w, P) - \rho_{bf}(P)V_{bf} \qquad (3)$$

where $n_{ex}(w, P)$ is the excess number of molecules in the simulation cell, $n_{abs}(w, P)$ is the simulated (absolute) number of molecules for the model pore of size H, ρ_{bf} (P) is the bulk fluid density at the different pressures and V_{bf} is the accessible volume for the bulk fluid.

In addition to the surface excess of adsorption, a thermodynamic quantity of interest that can be obtained form the GCMC is the isosteric enthalpy of adsorption. According to fluctuation theory [44]:

$$q_{iso} = \frac{\langle U\rangle\langle N\rangle - \langle UN\rangle}{\langle N^2\rangle - \langle N\rangle\langle N\rangle} + k_bT \qquad (4)$$

where $\langle\ldots\rangle$ is the ensemble average, k_b is the Boltzmann constant, N denotes the number of particles, and U is the configuration energy of the system.

The relation between isotherms determined by GCMC and the experimental isotherm on a porous solid can be interpreted in terms of a generalized adsorption isotherm (GAI) equation:

$$N(P) = \int N(P, w)f(w)dw \qquad (5)$$

where $N(P)$ is the experimental adsorption isotherm data, w is the pore width, $N(P, w)$ is the simulated isotherm on a single pore of width w, and $f(w)$ is the pore size distribution function.

The GAI equation reflects the assumption that the total isotherm consists of a number of individual "single pore" isotherms multiplied by their relative distribution, $f(w)$, over a range of pore sizes. The set of $N(P, w)$ isotherms (kernel) for this system was obtained by Monte Carlo computer simulation. The pore size distribution is then derived solving the GAI equation numerically via a fast non-negative least square algorithm. This is the most commonly used method to stabilize the result, incorporating additional constraints that are based on the smoothness of the PSD. This method, termed regularization, has been described in detail in several works [55–58]. In this work we used the procedure propose by Davies et al. [33,39].

Pore size distributions for the different gases have been calculated with kernels that contained pores with sizes between 4–36 Å for N_2, 4.13–11.25 Å for CO_2, 3.3–41 Å for H_2, 4.2–11.4 Å for CH_4 at low pressures and 4.2–38 Å for CH_4 at high pressures, see Refs. [23,33].

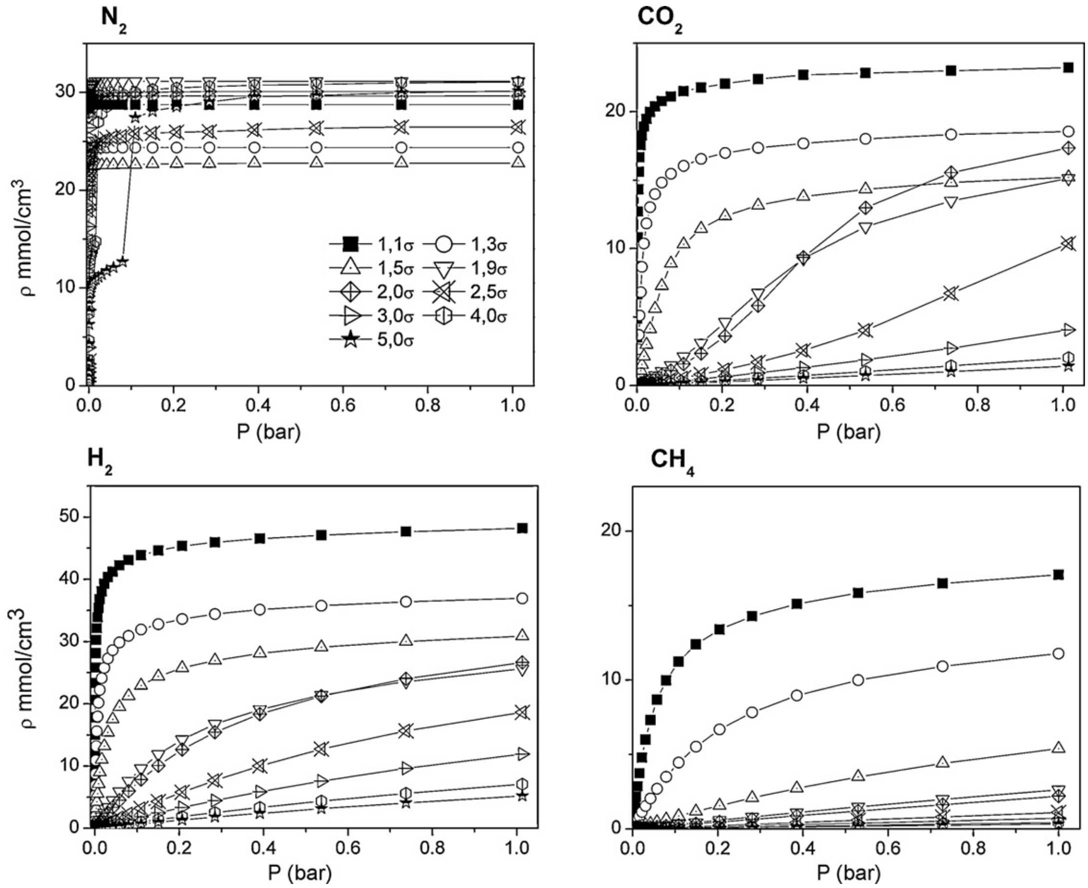

Fig. 2. Simulated gas adsorption isotherms for N_2 at 77 K, H_2 at 77 K, CO_2 at 273 K and CH_4 at 298 K for different pore sizes (pore sizes are expressed in terms of molecular diameters, σ, for each gas).

4. Results and discussion

Fig. 2 shows the simulated isotherms in a series of slit-shaped pores with different pore sizes for the different gases used in the study at low pressures (below 0.1 MPa or 1 bar). For a given gas, each isotherm corresponds to a defined pore size, which is determined in function of the molecular diameter of the individual gas (σ, Table 1). Adsorption takes place in such pores due to the enhanced adsorption potential between the pore walls. Adsorption in pores larger than a certain size becomes similar to that on a flat surface. Therefore, the adsorption isotherm becomes insensitive to the sizes of pores larger than a certain limiting value. As shown in Fig. 2 for the GCMC isotherms of H_2, the isotherms generated for pores larger than 10 Å (>3σ) become linearly dependent but they still contribute to the overall adsorption amount. This limit is similar in CO_2 isotherms, but in CH_4 it is no clear, because a lower adsorption occurs. For N_2, in the chosen range, this situation does not appear. Based on this observation, the integration limit in the calculation procedure should be extended above the sensitivity limit. It is important to realize that the proposed H_2 analysis can only be applied to characterize very small micropores.

Although the physisorbed gas can be a liquid, a solid or a 2D gas [59], a good approximation is to compare this density with the density of the studied gases in their liquid state (shown in Table 3), as reported by other authors [60,61]. In Fig. 2, we can see that all the gases, except methane, for adsorbents with determined pore sizes, can reach its liquid density in adsorbed state. Nitrogen and carbon dioxide are analyzed in sub-critical state while methane and hydrogen are analyzed in supercritical state. It is noticeable from these results that in porous materials with pores smaller than 1.3σ, hydrogen can be stored by an adsorption process reaching a density that cannot be achieved by another process. Another outstanding result is shown in the nitrogen simulated isotherms where the cell under study with the smallest pore size does not have the highest adsorption capacity as it would be expected. This is a recurrent effect up to 1.9σ and it might be associated to a configurational problem. This fact was highlighted in the literature as associated to nitrogen diffusion problems, but in GCMC simulations diffusion processes do not contribute to the filling of the pore, but this effect still appears.

Fig. 3 shows the experimental isotherms for all the prepared samples up to 0.1 MPa of pressure for the gases under study. All the samples show a similar behavior for the different gases, where progressive synthesis treatment improve their adsorption capacities, i.e., M40 < M40-20 < M40-28. For the gases with energetic applications, at the pressures studied, it can be observed that hydrogen is near to reach the plateau, but this is not so for methane, a behavior that requires further studies at high pressure.

Table 3
Density and critical temperature of the studied gases.

Molecule	T_c (K)[a]	ρ (mmol/cm^3)
CO_2	304.13	23.24[b]
CH_4	190.56	29.30[c]
H_2	32.97	35.12[d]
N_2	126.19	28.84[e]

[a] From Ref. [54].
[b] Density at 273 K, from Ref. [42].
[c] Density at 77 K, from Refs. [60,62].
[d] Density at 77 K, from Ref. [16].
[e] Density at 77 K, from Ref. [42].

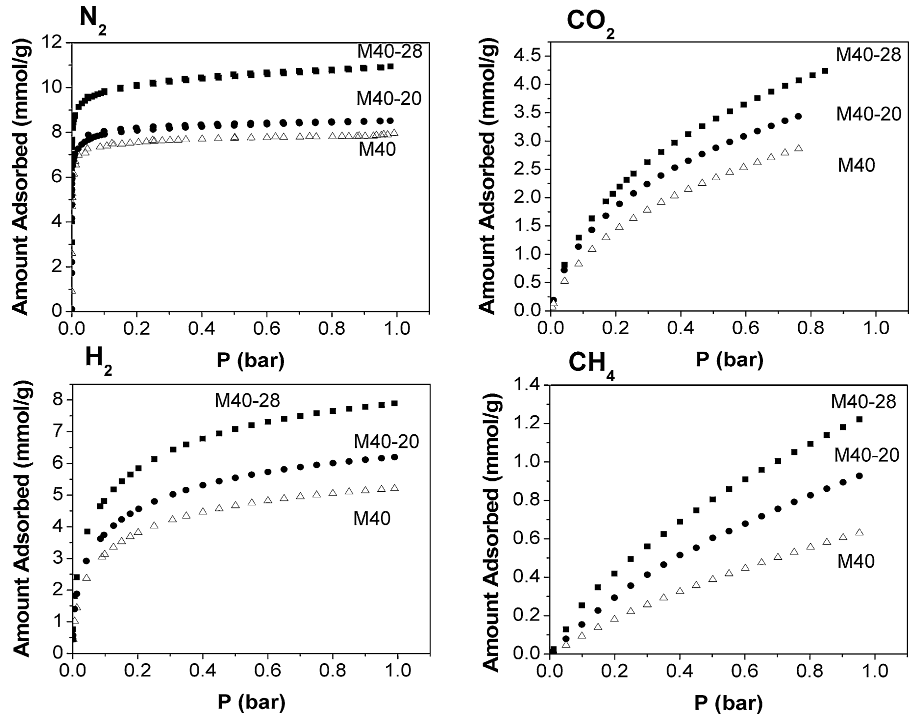

Fig. 3. Experimental gas adsorption isotherms for N_2 at 77 K, H_2 at 77 K, CO_2 at 273 K and CH_4 (low pressure) at 298 K.

Figs. 4–6 show the PSDs obtained for the samples using the different probe molecules. It is noticeable that: (i) the PSDs for the different gases and the same sample are different; and (ii) each gas presents a characteristic PSD for the different samples in a defined pore size range.

As already mentioned, H_2 only detects the smallest micropores (ultra-micropores), between 0.3 and 0.7 nm, while CO_2 detects a distribution between 0.4 and 1.2 nm for all the samples. The broadest PSD observed is for nitrogen and the narrowest for methane. In general there is good concordance between the PSDs obtained

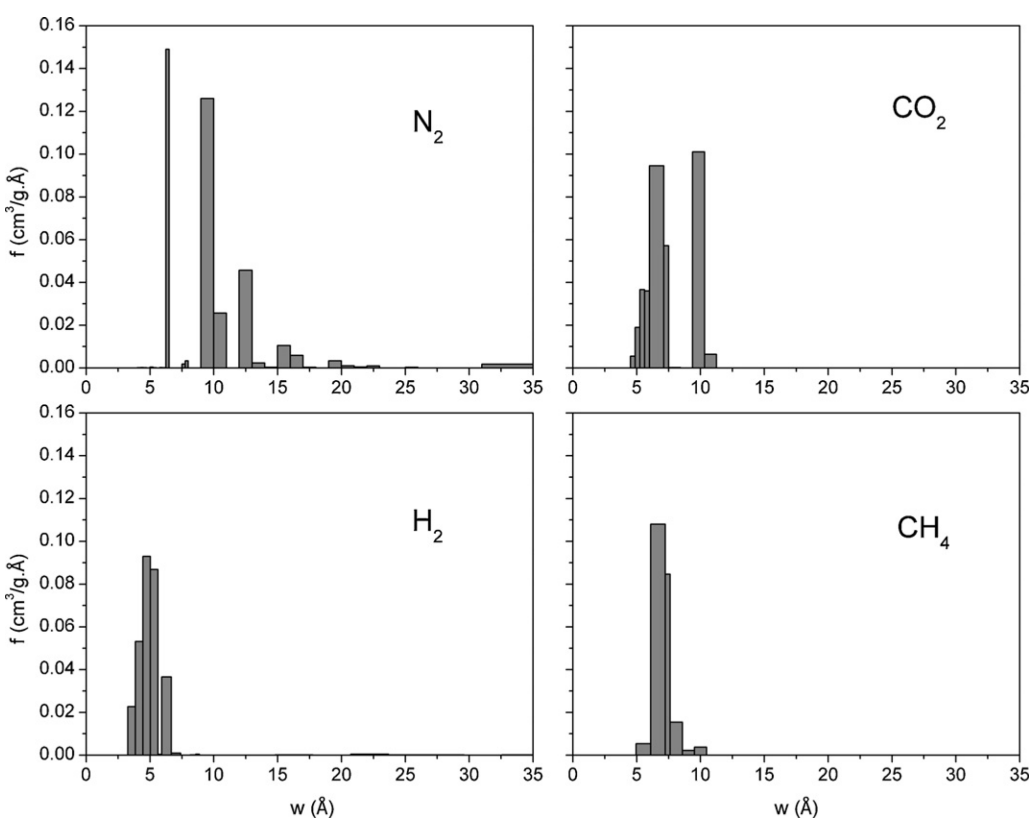

Fig. 4. PSDs of M40 activated carbon monolith obtained by GCMC simulation on H_2 at 77 K, CO_2 at 273 K, N_2 at 77 K and CH_4 at 298 K at pressures up to 0.1 MPa.

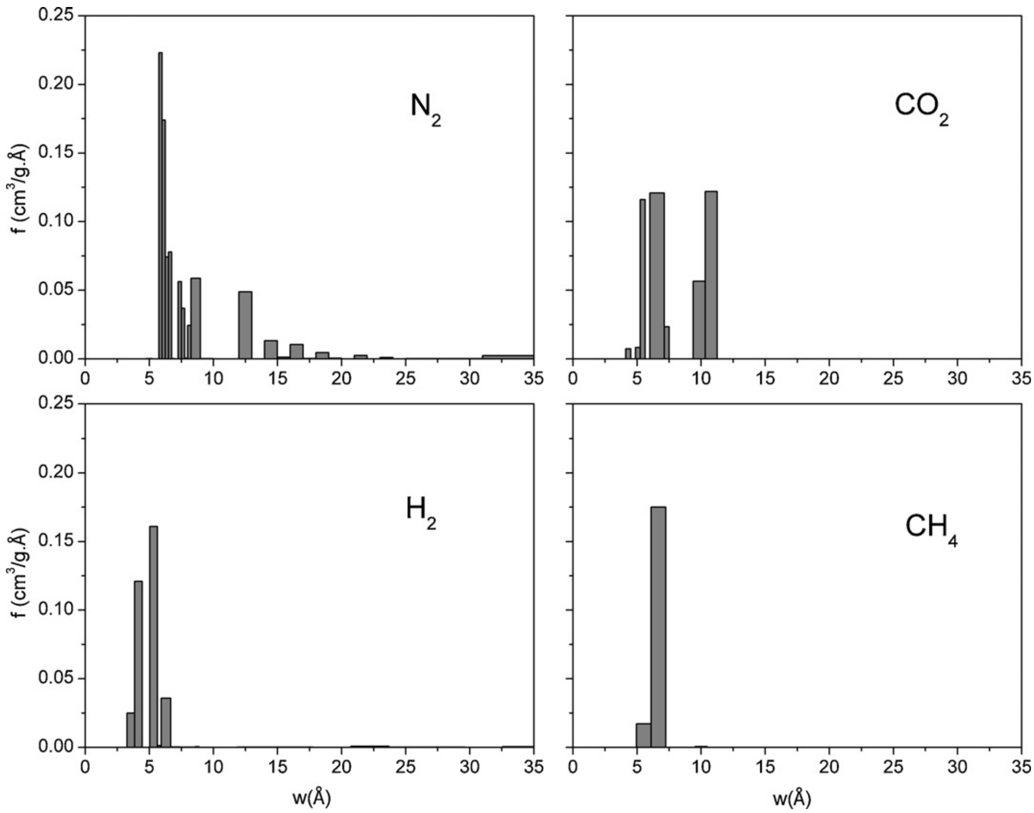

Fig. 5. PSDs of M40-20 activated carbon monolith obtained by GCMC simulation on H_2 at 77 K, CO_2 at 273 K, N_2 at 77 K and CH_4 at 298 K at pressures up to 0.1 MPa.

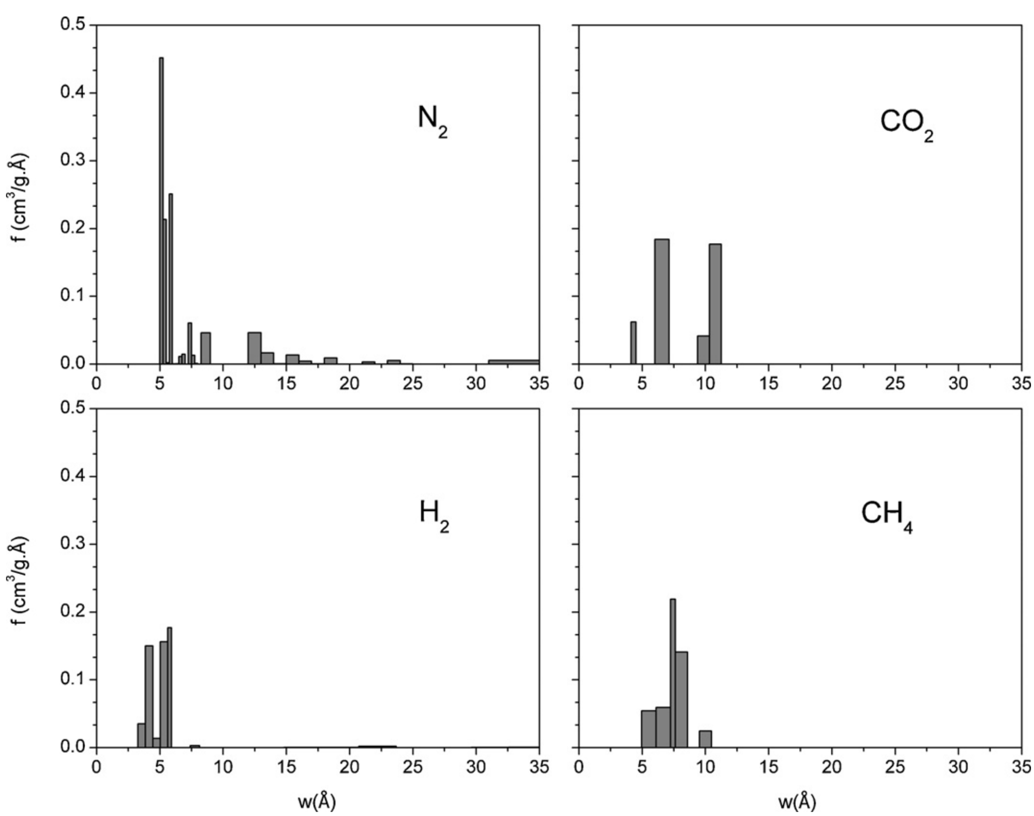

Fig. 6. PSDs of M4-28 activated carbon monolith obtained by GCMC simulation on H_2 at 77 K, CO_2 at 273 K, N_2 at 77 K and CH_4 at 298 K at pressures up to 0.1 MPa.

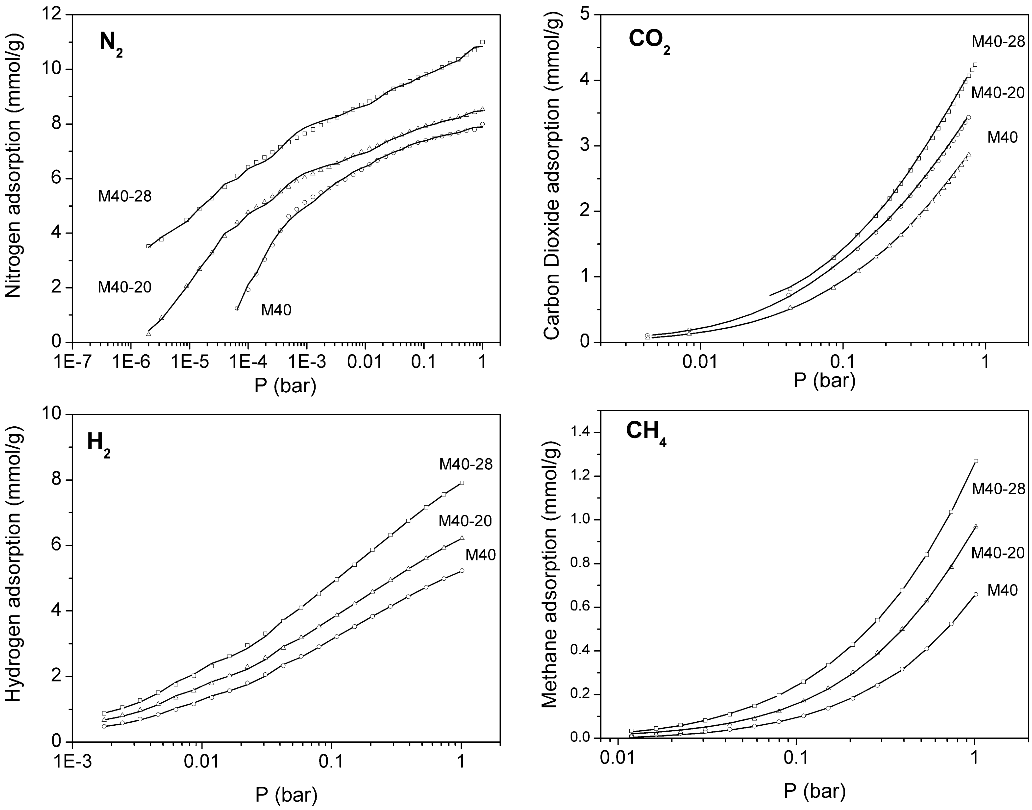

Fig. 7. Experimental (symbol) and fitted (line) isotherms for N_2 at 77 K, CO_2 at 273 K, H_2 at 77 K and CH_4 at 298 K from PSDs of Figs. 4–6.

using CO_2, N_2 and CH_4. They all detect pores between 0.6 and 0.9 nm.

Analyzing one gas at a time in Figs. 2–6, the results are consistent. For example, the experimental nitrogen isotherms show defined knees, corresponding to the simulated isotherms for pore sizes in all the range of analysis (Fig. 2). For CO_2 the shape of the experimental and simulated isotherms suggests that the pore size range is between 1.3σ and 3σ, as shown in PSD plots. In the methane adsorption studies it is clear that the distribution is sharper, with pore sizes in the range of 1.1σ to 1.9σ and for hydrogen the PSD is displaced to smaller pores, from 1.1σ to 2.5σ.

For the different samples and the same probe gas a similar PSD behavior is found. The successive activation processes (M40, M40-20, and M40-28) during the synthesis of monoliths produce a displacement of the PSD to smaller pores and an increment in the pore volumes, as it is observed in Figs. 4–6.

Fig. 7 presents, in logarithmic scale, the experimental and simulated isotherms resulting from the PSDs shown in Figs. 4–6, obtained with the different gases. For all the gases except nitrogen, the computed isotherms present a very good agreement with the experimental data, confirming the validity of the PSDs obtained. For the nitrogen case the agreement is acceptable, but a little deviation appears in the range of 1E−5 to 0.1 bars in pressure. This kind of deviations between the theoretical and the experimental isotherm (S-shaped) have been reported in the bibliography when sub-critical Ar or N_2 are used as probe gas to simulate adsorption in a perfect graphene-based slit pore [63,64]. The agreement between experimental and simulated isotherms is improved when defects

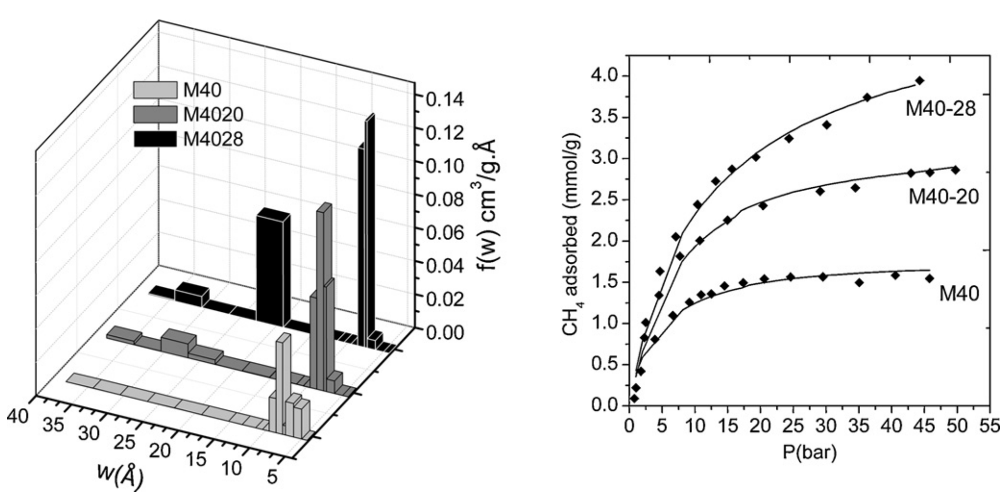

Fig. 8. Experimental (symbol) and fitted (line) methane adsorption isotherms and PSDs derived from high pressure methane isotherms for M40-0, M40-20 and M40-28.

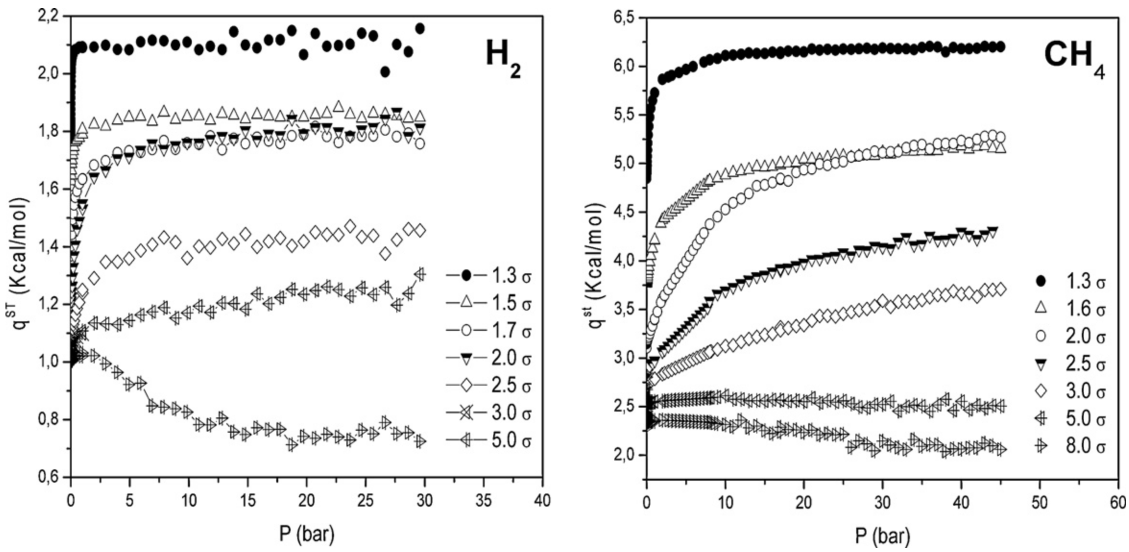

Fig. 9. Isosteric enthalpy of adsorption simulated by the GCMC method in slit-shaped pores of various effective widths for H_2 at 77 K (left) and CH_4 at 298 K (right).

Table 4
Micropore volumes calculated from semi-empirical models and from Monte Carlo simulation.

	N_2			CO_2		H_2	CH_4	HP-CH_4
	$V\mu p$ DR (cm^3/g)	$V\mu p$ α_s plot (cm^3/g)	$V\mu p$ MC (cm^3/g)	$V\mu p$ DR (cm^3/g)	$V\mu p$ MC (cm^3/g)	$V\mu p$ MC (cm^3/g)	$V\mu p$ MC (cm^3/g)	$V\mu p$ MC (cm^3/g)
M40	0.268	0.245	0.260	0.259	0.265	0.182	0.182	0.118
M40-20	0.276	0.260	0.290	0.269	0.362	0.214	0.220	0.188
M40-28	0.340	0.329	0.380	0.360	0.435	0.274	0.370	0.414

or geometric heterogeneity in the plates are considered, but this is subject of another work.

In Fig. 8 the studies for methane adsorption up to high pressures (up to 4.5 MPa) are presented. In this figure the experimental (symbols) and fitted (line) methane adsorption isotherms for all the pressure range are shown. Also the PSDs derived from high pressures are presented.

The predicted adsorption isotherms based on high pressure CH_4 PSDs are in very good agreement with experimental isotherms for the three samples, as shown in Fig. 8. The continuous increase in the adsorption isotherms at high pressure can be considered as evidence that an important contribution of the pores in the near-mesoporous region is developed in the samples M40-20 and M40-28, in coincidence with the PSDs obtained. In comparison to the PSDs at low pressure, there is a correspondence in the smallest microporous region for all the samples, but additional pore sizes are detected in near-mesoporous region for M40-20 and M40-28 at high pressure, which is consistent with the larger post-activation time used for these samples. In fact, these samples were post-activated for 3 h (M40-20) and 5 h (M40-28) in a carbon dioxide atmosphere developing some mesoporosity, which is only detected by high pressure CH_4 adsorption, indicating that this gas is more sensitive to mesopores near to the micropore region at these pressures. For the sample with the highest methane adsorption capacity (M40-28) these new peaks are in the range of 1.8–2.2 nm.

Fig. 9 presents the behavior of the configurational contribution to the isosteric heat of adsorption for CH_4 and H_2 adsorbed in slit pores of different sizes, obtained by GCMC. It can be seen how the heat decreases as the pore size increases, at any pressure. This also indicates that the attractive contribution of gas–gas interactions is stronger for the smallest pores where a more compact adsorbate structure can be formed.

Finally, the micropore volume for each sample was calculated using the simulated data and compared to the values obtained by standard methods like Dubinin–Radushchevich (DR) and α_s-plot (Table 4). Analyzing these data from the point of view of the sample preparation procedure, it is observed that all the methods indicate that the M40-28 sample is the most microporous material. For CO_2 and nitrogen, the standard methods give similar values and Monte Carlo simulations are consistent with these methods, but with higher values. It is clear that hydrogen and methane at low pressure detect only the small micropores, where the micropore volume is less than the measured for the other gases. Instead, the adsorption of methane at high pressure detects the presence of larger micropores, near the mesopore region, which is not seen for other gases at low pressures. Then, we can conclude that high pressure CH_4 adsorption is less sensitive to smaller pores and more sensitive to the larger ones, probably due to diffusive limitations in the high pressure region.

5. Conclusions

Results from the GCMC analysis obtained using different probe molecules at low pressures are consistent, which indicates that this method provides a mean for the reliable characterization of porous materials. The four calculated PSDs do not differ qualitatively and exhibit a limited use for the general prediction of adsorption behavior. On the other hand, the PSD of post-activated monoliths obtained from the GCMC analysis of CH_4 isotherms at high pressure, shows a peak around 20 Å (≈5σ), which is consistent with the development of pores in the near-mesoporous region developed by the post-activation process.

Additional information about micropores obtained from the CH_4 and H_2 analysis may be especially important for the characterization of materials considered for their application in energy storage systems. Although textural parameters provide an accessible and useful tool for an initial evaluation of activated carbons for the storage of natural gas and hydrogen, they do not always allow ranking these samples accurately. It was concluded that the textural parameters per se do not unequivocally determine methane and hydrogen storage capacities. Surface chemistry and gas adsorption equilibrium must be taken into account in the decision-making process of choosing the adsorbent for methane and hydrogen storage. Simultaneous adsorption and calorimetric experiments performed on the same sample should be extremely useful in order to carry out a more rigorous characterization. From these results it can be concluded that the use of different probes is essential for a reliable pore size analysis of these activated carbon monoliths.

Acknowledgements

The authors gratefully acknowledge CONICET (Consejo Nacional de Investigaciones Científicas y Técnicas) and ANPCyT (Agencia Nacional de Promoción Científica y Tecnológica) for the financial support to this research.

References

[1] V.C. Menon, S. Komarneni, Porous adsorbents for vehicular natural gas storage, J. Porous Mater. 5 (1998) 43–58.
[2] D. Lozano-Castelló, J. Alcañiz-Monge, M.A. de la Casa-Lillo, D. Cazorla-Amorós, A. Linares-Solano, Advances in the study of methane storage in porous carbonaceous materials, Fuel 81 (2002) 1777–1803.
[3] J.A.F. MacDonald, D.F. Quinn, Carbon absorbents for natural gas storage, Fuel 77 (1998) 61–64.
[4] J.W. Lee, H.C. Kang, W.G. Shim, C. Kim, H. Moon, Methane adsorption on multi-walled carbon nanotube at (303.15, 313.15, and 323.15) K, J. Chem. Eng. Data 51 (2006) 963–967.
[5] S.H. Yeon, S. Osswald, Y. Gogotsi, J.P. Singer, J.M. Simmons, J.E. Fischer, M.A. Lillo-Ródenas, M.A. Linares-Solano, Enhanced methane storage of chemically and physically activated carbide-derived carbon, J. Power Sources 191 (2009) 560–567.
[6] J.W. Lee, M.S. Balathanigaimani, H.C. Kang, W.G. Shim, C. Kim, H. Moon, Methane storage on phenol-based activated carbons at (293.15, 303. 15, and 313. 15) K, J. Chem. Eng. Data 52 (2007) 66–70.
[7] M.S. Balathanigaimani, M.J. Lee, W.G. Shim, J.W. Lee, H. Moon, Charge and discharge of methane on phenol-based carbon monolith, Adsorption 14 (2008) 525–532.
[8] J. Alcañiz-Monge, M.A. de la Casa-Lillo, D. Cazorla-Amoros, A. Linares-Solano, Methane storage in activated carbon fibres, Carbon 35 (1997) 291–297.
[9] S. Biloé, V. Goetz, S. Mauran, Characterization of adsorbent composite blocks for methane storage, Carbon 39 (2001) 1653–1662.
[10] N.D. Parkyns, D.F. Quinn, Natural gas adsorbed on carbon, in: J.W. Patrick (Ed.), Porosity in Carbons, Edwards Arnold, London, 1995, pp. 291–325.
[11] S. Biloé, V. Goets, A. Guillot, Optimal design of an activated carbon for an adsorbed natural gas storage system, Carbon 40 (2002) 1295–1308.
[12] F. Rodriguez-Reinoso, Y. Nakagawa, J. Silvestre-Albero, J.M. Suarez-Galán, M. Molina-Sabio, Correlation of methane uptake with microporosity and surface area of chemically activated carbons, Micropor. Mesopor. Mater. 115 (2008) 603–608.
[13] D. Lozano-Castelló, D. Cazorla-Amorós, A. Linares-Solano, D.F. Quinn, Influence of pore size distribution on methane storage at relatively low pressure: Preparation of activated carbon with optimum pore size, Carbon 40 (2002) 989–1002.
[14] R.F. Cracknell, P. Gordon, K.E. Gubbins, Influence of pore geometry on the design of microporous materials for methane storage, J. Phys. Chem. 97 (1993) 494–499.
[15] P. Bénard, R. Chahine, Determination of the adsorption isotherms of hydrogen on activated carbons above the critical temperature of the adsorbate over wide temperature and pressure ranges, Langmuir 17 (2001) 1950–1955.
[16] K.M. Thomas, Hydrogen adsorption and storage on porous materials, Catal. Today 120 (2007) 389–398.
[17] R. Ströbel, L. Jörissena, T. Schliermann, V. Trapp, W. Schütz, K. Bohmhammel, G. Wolf, J. Garche, Hydrogen adsorption on carbon materials, J. Power Sources 84 (1999) 221–224.
[18] M. Jordá-Beneyto, F. Suárez-García, D. Lozano-Castelló, D. Cazorla-Amorós, A. Linares-Solano, Hydrogen storage on chemically activated carbons and carbon nanomaterials at high pressures, Carbon 45 (2007) 293–303.
[19] M. Rzepka, P. Lamp, M.A. de la, Casa-Lillo, Physisorption of hydrogen on microporous carbon and carbon nanotubes, J. Phys. Chem. B 102 (1998) 10894–10898.
[20] I. Cabria, M.J. López, J.A. Alonso, The optimum average nanopore size for hydrogen storage in carbon nanoporous materials, Carbon 45 (2007) 2649–2658.
[21] P.I. Ravikovitch, G.L. Haller, A.V. Neimark, Density functional theory model for calculating pore size distributions: pore structure of nanoporous catalysts, Adv. Colloid Interface Sci. 76–77 (1998) 203–226.
[22] P.I. Ravikovitch, A.V. Neimark, Calculations of pore size distributions in nanoporous materials from adsorption and desorption isotherms, Stud. Surf. Sci. Catal. 129 (2000) 597–606.
[23] P.I. Ravikovitch, A. Vishnyakov, R. Russo, A.V. Neimark, Unified approach to pore size characterization of microporous carbonaceous materials from N_2, Ar, and CO_2 adsorption isotherms, Langmuir 16 (2000) 2311–2320.
[24] V.Y. Gusev, J.A. O'Brien, N.A. Seaton, A self-consistent method for characterization of activated carbons using supercritical adsorption and Grand Canonical Monte Carlo simulations, Langmuir 13 (1997) 2815–2821.
[25] Y. He, N.A. Seaton, Monte Carlo simulation and pore-size distribution analysis of the isosteric heat of adsorption of methane in activated carbon, Langmuir 21 (2005) 8297–8301.
[26] F. Rodriguez-Reinoso, A. Linares-Solano, Microporous structure of activated carbons as revealed by adsorption methods, in: P.A. Thrower (Ed.), Chemistry and Physics of Carbon, vol. 21, Marcel Dekker, New York, 1988.
[27] P.I. Ravikovitch, A. Vishnyakov, A.V. Neimark, M.M.L. Ribeiro Carrott, P.A. Russo, P.J. Carrott, Characterization of micro-mesoporous materials from nitrogen and toluene adsorption: experiment and modeling, Langmuir 22 (2006) 513–516.
[28] M. Konstantakou, Th.A. Steriotis, G.K. Papadopoulos, M. Kainourgiakis, E.S. Kikkinides, A.K. Stubos, Characterization of nanoporous carbons by combining CO_2 and H_2 sorption data with the Monte Carlo simulations, Appl. Surf. Sci. 253 (2007) 5715–5720.
[29] J. Jagiello, M. Thommes, Comparison of DFT characterization methods based on N_2, Ar, CO_2, and H_2 adsorption applied to carbons with various pore size distributions, Carbon 42 (2004) 1227–1232.
[30] S. Scaife, P. Kluson, N. Quirke, Characterization of porous materials by gas adsorption: do different molecular probes give different pore structures? J. Phys. Chem. B 104 (2000) 313–318.
[31] J. Jagiello, C.O. Ania, J.B. Parra, L. Jagiello, J.J. Pis, Using DFT analysis of adsorption data of multiple gases including H_2 for the comprehensive characterization of microporous carbons, Carbon 45 (2007) 1066–1071.
[32] H. Marsh, F. Rodríguez-Reinoso, Activated Carbon, Elsevier, London, 2006.
[33] G.M. Davies, N.A. Seaton, V.S. Vassiliadis, Calculation of pore size distributions of activated carbons from adsorption isotherms, Langmuir 15 (1999) 8235–8245.
[34] B. McEnaney, T.J. Mays, X. Chen, Computer simulations of adsorption processes in carbonaceous adsorbents, Fuel 77 (1998) 557–562.
[35] V.Y. Gusev, J.A. O'Brien, Can molecular simulations be used to predict adsorption on activated carbons? Langmuir 13 (1997) 2822–2824.
[36] S. Samios, A.K. Stubos, N.K. Kanellopulos, R.F. Cracknell, G.K. Papadopoulos, D. Nicholson, Determination of micropore size distribution from Grand Canonical Monte Carlo simulations and experimental CO_2 isotherm data, Langmuir. 13 (1997) 2795–2802.
[37] M.V. López-Ramón, J. Jagiello, T.J. Bandosz, N.A. Seaton, Determination of the pore size distribution and network connectivity in microporous solids by adsorption measurements and Monte Carlo simulation, Langmuir 13 (1997) 4435–4445.
[38] M.B. Sweatman, N.J. Quirke, Characterization of porous materials by gas adsorption at ambient temperatures and high pressure, J. Phys. Chem. B 105 (2001) 1403–1411.
[39] G.M. Davies, N.A. Seaton, The effect of the choice of pore model on the characterization of the internal structure of microporous carbons using pore size distributions, Carbon 36 (1998) 1473–1490.
[40] C. Almansa, M. Molina-Sabio, F. Rodríguez-Reinoso, Adsorption of methane into $ZnCl_2$-activated carbon derived discs, Micropor. Mesopor. Mater. 76 (2004) 185–191.
[41] D. Vargas, L. Giraldo, J.C. Moreno-Piraján, Y. Ladino, K. Sapag, Monoliths: synthesis and characterization using lignocellulosic precursor, in: Proceedings of the COPS VIII, 2009, pp. 167–173.
[42] J. Garrido, A. Linares-Solano, J.M. Martín-Martínez, M. Molina-Sabio, F. Rodriguez-Reinoso, R. Torregrosa, Use of N_2 vs. CO_2 in the characterization of activated carbons, Langmuir 3 (1987) 76–81.
[43] F. Rodriguez-Reinoso, J.M. Martin-Martinez, C. Prado-Burguete, B. McEnaney, A standard adsorption isotherm for the characterization of activated carbons, J. Phys. Chem. 91 (1987) 515–516.
[44] D. Nicholson, N.G. Parsonage, Computer Simulation and the Statistical Mechanics of Adsorption, Academic Press, London, 1982.
[45] W.A. Steele, The Interaction of Gases with Solid Surfaces, first ed., Pergamon, Oxford, UK, 1974.
[46] D. Cao, J. Wu, Modeling the selectivity of activated carbons for efficient separation of hydrogen and carbon dioxide, Carbon 43 (2005) 1364–1370.
[47] A. Vishnyakov, A.V. Neimark, Monte Carlo simulation test of pore blocking effects, Langmuir 19 (2003) 3240–3247.
[48] M. Heuchel, G.M. Davies, E. Buss, N.A. Seaton, Adsorption of carbon dioxide and methane and their mixtures on an activated carbon: simulation and experiment, Langmuir 15 (1999) 8695–8705.
[49] F. Roger, Cracknell, David Nicholson, Nicholas Quirke, A Grand Canonical Monte Carlo study of Lennard–Jones mixtures in slit shaped pores, Mol. Phys. 80 (1993) 885–897.
[50] D.L. Valladares, F. Rodríguez-Reinoso, G. Zgrablich, Characterization of active carbons: the influence of the method in the determination of the pore size distribution, Carbon 36 (1998) 1491–1499.
[51] D.Y. Peng, D.B. Robinson, A new two-constant equation of state, Ind. Eng. Chem. Fundam. 15 (1976) 59–64.

[52] U. Setzmann, W. Wagner, A new equation of state and tables of thermodynamic properties for methane covering the range from the melting line to 625 K at pressures up to 1000 MPa, J. Phys. Chem. 20 (1991) 1061–1151.
[53] R. Span, W. Wagner, A new equation of state for carbon dioxide covering the fluid region from the triple-point temperature to 1100 K at pressures up to 800 MPa, J. Phys. Chem. 25 (1996) 1509–1596.
[54] S.I. Sandler, Chemical and Engineering Thermodynamics, third ed., Wiley, New York, 1989.
[55] J.D. Wilson, Statistical approach to the solution of first-kind integral equations arising in the study of materials and their properties, J. Mater. Sci. 27 (1992) 3911–3924.
[56] M.V. Szombathely, P. Brauer, M. Jaroniec, The solution of adsorption integral equations by means of the regularization method, M.J. Comput. Chem. 13 (1992) 17–32.
[57] P.H. Merz, Determination of adsorption energy distribution by regularization and a characterization of certain adsorption isotherms, J. Comput. Phys. 38 (1980) 64–85.
[58] G. Whaba, Practical approximate solutions to linear operator equations when the data are noisy, SIAM J. Numer. Anal. 14 (1977) 651–667.
[59] F. Rouquerol, J. Rouquerol, K. Sing, Adsorption by Powders and Porous Solids, Academic Press, London, 1999.
[60] D.D. Do, H.D. Do, Adsorption of supercritical fluids in non-porous and porous carbons: analysis of adsorbed phase volume and density, Carbon 41 (2003) 1777–1791.
[61] P. Kowalczyk, H. Tanaka, K. Kaneko, A.P. Terzyk, D.D. Do, Grand Canonical Monte Carlo simulation study of methane adsorption at an open graphite surface and in slitlike carbon pores at 273 K, Langmuir 21 (2005) 5639–5646.
[62] A.W. Francis, Pressure–temperature–liquid density relations of pure hydrocarbons, Ind. Eng. Chem. 49 (1957) 1779–1786.
[63] J.P. Olivier, Improving the models used for calculating the size distribution of micropore volume of activated carbons from adsorption data, Carbon 36 (1998) 1469–1472.
[64] A.V. Neimark, Y. Lin, P.I. Ravikovitch, M. Thommes, Quenched solid density functional theory and pore size analysis of micro–mesoporous carbons, Carbon 47 (2009) 1617–1628.